
Article:
Bellasio, C., Beerling, D.J. and Griffiths, H. (2016) Deriving C4 photosynthetic parameters from combined gas exchange and chlorophyll fluorescence using an Excel tool: theory and practice. Plant, Cell & Environment, 39 (6). pp. 1164-1179. ISSN 0140-7791

https://doi.org/10.1111/pce.12626

Plant, Cell and Environment

Deriving C_4 photosynthetic parameters from combined gas exchange and chlorophyll fluorescence using an Excel tool: theory and practice

Chandra Bellasio[1*], David J Beerling[1] and Howard Griffiths[2]

1 Department of Animal and Plant Sciences, University of Sheffield, Sheffield, S10 2TN, UK

2 Department of Plant Sciences, University of Cambridge, Cambridge, CB2 3EA, UK

*Correspondence: c.bellasio@sheffield.ac.uk

This article has been accepted for publication and undergone full peer review but has not been through the copyediting, typesetting, pagination and proofreading process, which may lead to differences between this version and the Version of Record. Please cite this article as doi: 10.1111/pce.12626

Abstract:

The higher photosynthetic potential of C_4 plants has led to extensive research over the past 50 years, including C_4–dominated natural biomes, crops such as maize, or for evaluating the transfer of C_4 traits into C_3 lineages. Photosynthetic gas exchange can be measured in air or in a 2% Oxygen mixture using readily available commercial gas exchange and modulated PSII fluorescence systems. Interpretation of these data, however, requires an understanding (or the development) of various modelling approaches, which limit the use by non–specialists. In this paper we present an accessible summary of the theory behind the analysis and derivation of C_4 photosynthetic parameters, and provide a freely available Excel Fitting Tool (EFT), making rigorous C_4 data analysis accessible to a broader audience. Outputs include those defining C_4 photochemical and biochemical efficiency, the rate of photorespiration, bundle sheath conductance to CO_2 diffusion, and the in vivo biochemical constants for PEP carboxylase. The EFT compares several methodological variants proposed by different investigators, allowing users to choose the level of complexity required to interpret data. We provide a complete analysis of gas exchange data on maize (as a model C_4 organism and key global crop) to illustrate the approaches, their analysis and interpretation.

Keywords

Modelling, quantum yield, respiration, compensation point, ATP production, photorespiration, PEP, PEPC, oxygenation, carboxylation, Rubisco, specificity, bundle sheath conductance, C_{BS}.

Running title

Analysis of C_4 gas exchange data

Introduction

Although accounting for a relatively small number of species (c. 7500), C_4 plants have disproportionate ecological, economic, and strategic importance. In fact, they dominate various biomes across the planet, contributing to 25% of the total terrestrial net productivity (Osborne & Beerling, 2006, Sage & Stata, 2015), while C_4 crops such as maize, sugarcane, and sorghum lead the world grain, sugar, and biofuel production (faostat.fao.org). C_4 photosynthesis has high production potential in warm climates and, consequently, considerable effort has been made to explore the possibility of transferring beneficial C_4 traits to improve C_3 crop productivity and yield over recent years (Hibberd et al., 2008, Long et al., 2015, Singh et al., 2014, von Caemmerer et al., 2012). C_4 photosynthesis results from biochemical and anatomical modifications of the leaf parenchyma. External mesophyll (M; symbols and acronyms are listed in Table 1) cells and internal bundle sheath (BS) cells are coupled to operate a biochemical carbon concentrating mechanism (CCM). CO_2 is initially fixed by phosphoenolpyruvate (PEP) carboxylase (PEPC) and converted into C_4 (amino)acids. These diffuse to the BS where CO_2 is released, a process that increases CO_2 concentration in the BS, the cellular compartment where Rubisco is exclusively expressed. Despite a notable direct metabolic cost resulting from the ATP required to regenerate PEP, the CCM actively suppresses the oxygenase activity of Rubisco and consequently reduces the energy costs associated with photorespiratory metabolite recycling (Bellasio & Griffiths, 2014a).

Whether comparing natural vegetation or manipulated plants, it is essential to quantify the performance of C_4 photosynthesis across contrasting decarboxylase subgroups or under controlled and natural environmental conditions. This generally involves gas exchange measurements and photosynthetic modelling. Leaf photosynthetic CO_2 uptake (referred to as net assimilation, A), water vapour transpiration, and leaf–level fluorescence yield (F) can be measured with modern Portable Fluorescence–Gas Exchange systems (GES). GES software uses classical calculations (Genty et al., 1989, von Caemmerer & Farquhar, 1981) to derive stomatal conductance to H_2O, and then CO_2 (g_S), the CO_2 concentration in the substomatal cavity (C_i), and the photochemical yield of PSII (Y(II)). Gas exchange techniques can be augmented if a low O_2 (2%) mixture is fed to the GES cuvette instead of air. GES outputs can be used iteratively to inform photosynthetic models using 'curve fitting' [recently reviewed in (Bellasio et al., 2015)], finding parameter values that best characterise the response of a given plant. These parameters are convenient proxies, which may mechanistically represent the underpinning biochemical traits or empirically summarise the dataset, and can be interrogated statistically to characterise differences between plants or experimental treatments.

We have recently developed such curve fitting and fast screening tools, (Bellasio et al., 2015, Bellasio et al., 2014a) based on the assumption that photosynthesis is limited by NADPH and, because the NADPH requirements are the same for all photosynthetic types, they are of general use for natural vegetation, cultivated varieties, or plants with engineered photosynthetic traits. By estimating the relative engagement of the reductive pentose phosphate (RPP) and photosynthetic carbon oxygenation (PCO) cycles (as the Rubisco rate of oxygenation vs carboxylation, V_O/V_C), plants may be assigned to photosynthetic types (C_3, C_3–C_4, C_2, C_4). For full C_4 traits, we now refine the analysis of Bellasio et al. (2015), to derive quantities typical for C_4 metabolism (e.g. the PEP carboxylation rate, V_P), using a specific C_4 model.

Several biochemical models of C_4 photosynthesis have been proposed that define gas exchange characteristics of leaves and simulate the operation of the CCM (Berry and Farquhar, 1978; Laisk and Edwards, 2009; Laisk and Edwards, 2000; von Caemmerer, 2000). Earlier approaches were joined into the von Caemmerer (2000) C_4 model (hereafter C_4 model), which has two different formulations: 1) the enzyme–limited formulation, underpinned by the kinetics of PEPC and Rubisco; and 2) the light–limited formulation, based on the assumption that, under limiting light, C_4 photosynthesis is solely limited by the total rate of ATP production (J_{ATP}). Because of its complexity, C_4 modelling has been traditionally confined to specialist literature, and there is a timely need to make data analysis modelling tools available to a broader audience.

Here we present an Excel fitting tool (EFT) which derives a suite of C_4 photosynthetic parameters and predicts variables of the C_4 model, describe the theory of C_4 modelling and data analysis and succinctly demonstrate a range of applications with a worked example using maize. We have developed a C_4 EFT using the same rationale as that for C_3 plants (Bellasio et al., 2015): 1) the EFT and the example dataset are freely available to download from Supporting Materials; 2) the use of macros is avoided, allowing greater transparency and straight–forward modification; 3) the EFT accommodates a wide range of methodological variations for more advanced applications. Besides parameter fitting sub–routines, the EFT codes the equations for predicting the CO_2 concentration in M and BS (and associated quantities), which can be used in isotopic modelling, but this is not discussed further in this paper (Bellasio & Griffiths, 2014b, Cernusak et al., 2013, Ubierna et al., 2011, von Caemmerer et al., 2014). The EFT calculates some basic biochemical quantities (e.g. rate of photorespiration), which can underpin more sophisticated stoichiometric derivation (Bellasio & Griffiths, 2014c). In this paper we detail the rationale of the different formulations of the C_4 model with a step–by–step, logical approach. In the second part of this

paper, a worked analysis of gas exchange data measured on maize plants exemplifies how the outputs from the EFT allow a detailed characterisation of C_4 photosynthesis.

Theoretical underpinnings of the EFT

To take advantage of the full functionality of the EFT, light and A/C_i curves measured under ambient and low O_2 are required for each plant. All four curves are measured sequentially on the same portion of the leaf (see details in the worked example below). When curves are measured on different leaves, or at different times, they have to be treated as independent. In this case, and if any of the four curves are unavailable, it is still possible to use the EFT, although with more limited functionality (see Partial datasets below). The rationale for repeating measurements under low O_2 (2 – 5%) is to suppress photorespiration. Under these conditions a relationship between Y(II) and J_{ATP} can be assumed [(Bellasio & Griffiths, 2014b, Yin et al., 2011b), but see Discussion] and then used to estimate J_{ATP} under ambient O_2. The O_2 level needs to be sufficient to drive mitochondrial respiration and to avoid overreduction of the plastoquinone pool, and mixtures with 2% or 5% O_2 are generally regarded as an optimal compromise (Maroco et al., 1998).

We propose a logical protocol similar to that previously described (Bellasio et al., 2015) whereby data analysis is divided into 13 discrete steps (EFT sheets are numbered 1 – 13 accordingly) and each step extracts a new piece of information using parameters previously derived. The C_4 equations implemented here were taken from (Bellasio & Griffiths, 2014b, Ubierna et al., 2011, von Caemmerer, 2000, Yin et al., 2011b), or originally derived for this current work (see detailed description of each step). Steps 1, 3, 4, and 5 are identical to Bellasio et al. (2015), however, to avoid confusion and for completeness, we include a brief description of these steps. The 13 steps are summarised as follows:

1 Data are entered into the EFT and limitations are manually selected.

2 Respiration in the light (R_{LIGHT}) is derived using the initial light–limited portion of the fluorescence–light–curves (Yin et al., 2011b).

3 The initial yield of photosystem II ($Y(II)_{LL}$) is extrapolated under zero PPFD by linear, quadratic, or exponential regression of Y(II) in the initial light–limited portion of the fluorescence–light–curves.

4 Gross assimilation (GA) is calculated by summing R_{LIGHT} plus A, and the PPFD dependence of GA is described empirically by a non–rectangular hyperbola. The maximum quantum yield for CO_2 fixation ($Y(CO_2)_{LL}$) and the light–saturated GA (GA_{SAT}) are estimated by curve–fitting. The light compensation point (LCP) is calculated from the fitted curve.

5 An empirical non–rectangular hyperbola is fitted to the A/C_i curves under ambient and low O_2 to estimate the maximal carboxylating efficiency (CE), the C_i–A compensation point (Γ), and CO_2–saturated A (A_{SAT}). Stomatal limitation (L_S) is assessed using the fitted curve in analogy to the graphical method (Farquhar & Sharkey, 1982).

6 A calibration factor to calculate J_{ATP} is derived using two different approaches: the approach of Yin (Yin et al., 2011b) (output as a quantity called s′) and an approach originally derived in this work by analogy to that of Valentini (Valentini et al., 1995) (output as a quantity called k′).

7 With $Y(II)_{LL}$ and either s′ or k′, the initial quantum yield for ATP production ($Y(J_{ATP})_{LL}$, the conversion efficiency of PPFD into J_{ATP}) is calculated.

8 J_{ATP} is calculated using PPFD, Y(II), and s′ or k′ derived in Step 7, or with a point–to–point approach directly from GA (Bellasio & Griffiths, 2014b).

9 The light–dependence of J_{ATP} under ambient O_2 is described by an empirical non–rectangular hyperbola. With $Y(J_{ATP})_{LL}$ (derived in Step 7) defining the initial slope, the curvature (θ) and light–saturated J_{ATPSAT} are estimated by curve–fitting.

10 J_{ATP} is modelled (J_{ATPMOD}) upon measured A and C_i, and R_{LIGHT} derived in Step 2, using the light limited equations of C_4 photosynthesis (Ubierna et al., 2013). Bundle sheath conductance to CO_2 diffusion (g_{BS}) is estimated by fitting J_{ATPMOD} to empirical values of J_{ATP} (calculated in Step 8) in the light–limited part of light–curves and A/C_i curves [this curve fitting is referred to as the 'J/J' approach (Bellasio & Griffiths, 2014b), calculation variants are available].

11 With g_{BS} derived in Step 10, assimilation is modelled (A_{MOD}) in the enzyme–limited part of the A/C_i curve. In vivo V_{PMAX} (PEPC CO_2 saturated rate) and K_P (PEPC Michaelis–Menten constant for CO_2) are estimated by fitting A_{MOD} to A, in the enzyme–limited portion of A/C_i curves (calculation variants are available, including the possibility to fit low O_2 A/C_i curves).

12 With A, C_i, g_{BS} (derived in Step 10), and J_{ATP} (calculated in Step 8), the Rubisco rate of carboxylation (V_C), Rubisco rate of oxygenation (V_O), and PEPC rate of carboxylation (V_P) are calculated.

13 The CO_2 leak rate L, leakiness (ϕ), the CO_2 concentration in M (C_M), the CO_2 concentration in BS (C_{BS}), and the O_2 concentration in BS (O_{BS}) are estimated for each point of the A/C_i and light curves using the equations of the C_4 model (von Caemmerer, 2000) (calculation variants are available).

For clarity, we note that here we used a purely biochemical notation, but often anatomical notation is used to qualify biochemical variables (e.g. ‘m’ to identify PEP regeneration or ‘s’, for BS, to identify PCO and RPP cycles) and may lead to some ambiguity. Note that the C_4 model does not provide information on where processes occur and, in order to acquire information on biochemical compartmentalisation, a more complex modelling approach is required (Bellasio & Griffiths, 2014c, McQualter et al., 2015, Wang et al., 2014). Next we describe the practical use of the EFT, together with theory and possible alternatives following the step–by–step procedure.

1. Data entry and selection of limitations

For each datapoint of the four response curves, PPFD, A, C_i, and Y(II) are entered in Sheet 1 as the outputs from GES software, corrected for leaf cuvette gasket CO_2 diffusion when appropriate (Bellasio et al., 2015). The datasets are automatically plotted graphically below the tables. A colour code is maintained throughout the EFT: brown is used to indicate ambient O_2 conditions, while blue refers to low O_2. Modelled functions appear as continuous lines, modelled points appear as crosses, grey cells contain general output and white cells require data input. The data entered in Sheet 1 will be automatically transferred to subsequent sheets in cells with a light–shaded background: for the sake of flexibility these cells can be overwritten by the user (see also Partial datasets below).

Along with each datapoint, a limitation code (1, 2 or 3) is required, which identifies the datapoints to be used in subsequent analyses and manipulations. For light–curves, ‘1’ is assigned to the initial light–limited points, ‘2’ to the light–limited points, and ‘3’ to the remainder of the points. For A/C_i curves ‘1’ is assigned to the initial PEPC–limited part of the curve, ‘2’ to the PEPC–limited part of the curve, and ‘3’ to the light–limited part of the curve (a worked example is provided in the second part of this paper). Each fitting step is largely independent of the others, meaning that limitations can be adjusted between one step and the next and individual datapoints can be excluded from further analysis (see instructions in Sheet 1).

2. Estimating respiration in the light (R_{LIGHT})

The definition and importance of R_{LIGHT}, and the available methods for R_{LIGHT} estimation have been reviewed previously (Bellasio et al., 2015). Methods based on A/C_i curve analysis such as the Laisk method and the method of Brooks and Farquhar (Brooks & Farquhar, 1985) cannot be used for C_4 plants (Yin et al., 2011a). Here we implemented the C_4 variant of the fluorescence–light curve method proposed by Yin (Yin et al., 2011b). Assimilation is plotted

against 1/3 Y(II) PPFD yielding a linear relationship, and R_{LIGHT} is independently estimated under low and ambient O_2 as the y–intercept of the fitted line:

$$A = s' {}^{1}/_{3}\ Y(II)\ PPFD\ - R_{\mathrm{LIGHT}}, \quad (1)$$

where s′ is a lumped conversion coefficient (see Step 6).

This gas exchange–chlorophyll fluorescence method has been experimentally validated for C_4 plants (Bellasio & Griffiths, 2014b, Yin et al., 2011b). Note that the estimate for R_{LIGHT} is obtained under low PPFD and the independence of R_{LIGHT} from PPFD is assumed. The derivation of R_{LIGHT} in Sheet 2 was separated from the derivation of s′ in Sheet 6a to allow additional features in Sheet 2, including the possibility to add additional data to the regressions (the light–limited part of the A/C_i curve and R_{DARK}, measured under ambient and/or low O_2), and the possibility of a single value for R_{LIGHT}-fitted to pooled ambient and low O_2 data, since in practical terms, any O_2 effect may be considered negligible (Yin et al., 2009).

3. Initial photochemical yield of PSII ($Y(II)_{LL}$)

$Y(II)_{LL}$ represents the initial (and maximal) photochemical yield of PSII obtained under conditions of steady state illumination and accounts for conversion losses occurring under operational conditions. Based on the observation that Y(II) increases monotonically at decreasing PPFD (Yin et al., 2014), Sheet 3 calculates $Y(II)_{LL}$ as the y–intercept of a function fitted to Y(II) plotted against PPFD. Alongside linear fitting, additional features in Sheet 3 allow comparison with quadratic and exponential functions, fitted to several combinations of datapoints.

4. Light dependence of gross assimilation (GA), light–saturated gross assimilation (GA_{SAT}), initial quantum yield for CO_2 fixation ($Y(CO_2)_{LL}$), and light compensation point (LCP)

The dependence of GA on PPFD can be modelled empirically as:

$$GA_{MOD} = \frac{Y(CO_2)_{\mathrm{LL}}\ PPFD + GA_{\mathrm{SAT}} - \sqrt{(Y(CO_2)_{\mathrm{LL}}\ PPFD + GA_{\mathrm{SAT}})^2 - 4\ m\ Y(CO_2)_{\mathrm{LL}}\ PPFD\ GA_{\mathrm{SAT}}}}{2\ m}. \quad (2)$$

Eqn 2 is a non–rectangular hyperbola parameterised by GA_{SAT}, $Y(CO_2)_{LL}$, and m, an empirical factor ($0 \leq m \leq 1$) defining the curvature. GA_{SAT} defines the horizontal asymptote ($GA=GA_{SAT}$) and represents the light–saturated rate of GA under the CO_2 concentration used for measurements. $Y(CO_2)_{LL}$ corresponds to the maximal quantum yield for CO_2 fixation ($Y(CO_2)$ i.e. the conversion efficiency of PPFD into fixed CO_2, often referred to as Φ_{CO2}) and defines the inclined asymptote ($GA=Y(CO_2)_{LL}$ PPFD). To facilitate the physiological interpretation of m, Sheet 4 calculates the PPFD which half saturates GA ($PPFD_{50}$), analogous to a $K_{1/2}$ kinetic parameter. The values of $Y(CO_2)_{LL}$, m, and GA_{SAT} are found by iterative fitting of GA_{MOD} to GA. These parameters can readily be used to highlight phenotypic variations. A recently proposed linear alternative for the derivation of $Y(CO_2)_{LL}$ (Yin et al., 2014) can be compared in the additional features of Sheet 6a. From Sheet 4a onwards, we have included the possibility to log–transform residuals. By partially correcting for proportionality between residuals and modelled quantity (e.g. GA), this feature increases the weight of initial datapoints (e.g. low PPFD) in determining the characteristics of the fitted curve. The opportunity to log–transform depends on the characteristics of the dataset and the structure of error and should be considered on a case–by case basis.

The fitted hyperbola is used to calculate the PPFD–A compensation point, LCP [the importance of which has been reviewed in (Bellasio et al., 2015)] by solving Eqn 2 for PPFD under the condition of A=0, i.e. $GA=R_{LIGHT}$. A linear alternative to derive LCP from the initial region of the light–response curve can be compared in the additional features of Sheet 3.

5. CO_2 dependence of assimilation (A), CO_2–saturated assimilation (A_{SAT}), initial carboxylating efficiency for CO_2 fixation (CE), C_i–A compensation point (Γ), and stomatal limitation (L_S)

The relationship between A and C_i can be modelled mechanistically to derive important PEPC kinetic parameters (Step 11), however, important information can also be acquired by empirical modelling without the need for any particular physiological constraint (Bellasio et al., 2015). Assimilation can be modelled in terms of C_i through a non–rectangular hyperbola (analogous to Eqn 2):

$$A_{\mathrm{MOD}} = \frac{CE\,(C_i-\Gamma)+A_{\mathrm{SAT}}-\sqrt{(CE\,(C_i-\Gamma)+A_{\mathrm{SAT}})^2-4\,\omega\,CE\,(C_i-\Gamma)\,A_{\mathrm{SAT}}}}{2\,\omega}. \quad (3)$$

Eqn 3 is calculated in sheets 5a and 5b and is parameterised by A_{SAT}, CE, Γ, and ω. A_{SAT} represents the CO_2–saturated rate of A under the PPFD of the measurement, and is the

horizontal asymptote ($A=A_{SAT}$). CE is known as maximal carboxylating efficiency for CO_2 fixation (CE), and defines the inclined asymptote, which has the equation $A=CE\ (C_i–\Gamma)$, i.e. the asymptote equation corresponds to the linear equation of (Farquhar & Sharkey, 1982). ω is an empirical factor ($0\leq \omega \leq 1$) defining curvature. To facilitate the physiological interpretation of ω, sheets 5a and 5b calculate the C_i which half saturates A (C_{i50}) – analogous to a $K_{1/2}$ kinetic parameter. With R_{LIGHT} derived in Step 2, the values of CE, ω, Γ, and A_{SAT} are found by iterative fitting of A_{MOD} to measured A.

The fitted equation can be useful to assess stomatal limitation (L_S) imposed by stomatal conductance (g_S) analogous to previous graphical methods (Farquhar & Sharkey, 1982, Long & Bernacchi, 2003). Stomatal limitation L_S is generally assessed by comparing a value of assimilation rate A′ measured under ambient CO_2 concentration (i.e. when $C_i = C_a - \frac{A}{g_S}$) with the hypothetical A″ that would be obtained if the mesophyll had free access to the CO_2 in the ambient air (i.e. when $C_i=C_a$). In Sheet 5a, by specifying C_a and C_i, stomatal limitation can be calculated under any CO_2 concentration, this may be useful when comparing plants grown under contrasting CO_2 concentrations. Sheet 5a calculates L_S as:

$$L_S = \frac{A'' - A'}{A''}, \qquad 4$$

where A′ is calculated by solving Eqn 3 for the specified C_i and A″ is calculated by solving Eqn 3 for the specified C_a.

6. A calibration factor to calculate J_{ATP}

A calibration factor to calculate J_{ATP} is derived for each individual plant using the data obtained under low O_2 conditions (Bellasio et al., 2015), where the ATP cost of GA can be assumed (see steps 7 and 8, and Discussion). In the EFT we implemented two approaches: the approach of Yin et al. (2011b) and an approach modified from Valentini et al. (1995).

The Yin approach is based on Eqn 1, and the y–intercept, R_{LIGHT}, was derived in Sheet 2. The slope s′ is derived in Sheet 6a. s′ is a conversion coefficient lumping the fraction of PPFD harvested by PSII with several other difficult to measure quantities (Yin & Struik, 2012), such as leaf absorptance, PSII optical cross–section, stoichiometry of the ATP synthase, engagement of cyclic electron flow, and alternative electron pathways (Yin et al., 2004).

Alternatively, in Sheet 6b, modified from the approach of Valentini, an empirical linear relationship between $Y(CO_2)$ and Y(II) is fitted:

$$Y(II) = k' Y(CO_2) + b, \quad 5$$

where Y(II) is measured directly and $Y(CO_2)$ is calculated as $\frac{GA}{PPFD}$, k′ is the slope and b is the intercept of the fitted line. b represents the fraction of Y(II) not used by C_4, RPP and PCO cycles.

7. Initial quantum yield for ATP production ($Y(J_{ATP})_{LL}$)

The initial quantum yield for ATP production ($Y(J_{ATP})_{LL}$) is the maximal conversion efficiency of incident light into ATP, mathematically extrapolated to PPFD=0. In Sheet 6a, with the calibration of Yin, $Y(J_{ATP})_{LL}$ is calculated as:

$$Y(J_{\mathrm{ATP}})_{\mathrm{LL}} = \frac{s\prime\, Y(II)_{\mathrm{LL}}}{1-x}, \quad 6$$

where $Y(II)_{LL}$ was derived by linear, quadratic, or exponential fits in Step3 and x is the fraction of J_{ATP} used for PEP regeneration under low O_2 [generally assumed 0.4, e.g. (Ubierna et al., 2013)].

In Sheet 6b $Y(II)_{LL}$ is calculated modified from the Valentini approach:

$$Y(J_{ATP})_{\mathrm{LL}} = \frac{5}{k\prime}\ (Y(II)_{\mathrm{LL}} - b), \quad 7$$

where 5 is the ATP requirement for GA under low O_2 (different values can be specified in the EFT, see Discussion), and can be related to the approach of Yin as $5 = \frac{3}{1-x}$ (Eqn 1 and 7).

8. Rate of ATP production (J_{ATP})

J_{ATP} is the total ATP production rate used by photosynthetic processes (PEP regeneration, RPP and PCO cycles) and does not include alternative ATP sinks. These are excluded for consistency with the assumptions in subsequent derivations (i.e. rates of PEP carboxylation and rates of RuBP oxygenation and carboxylation, see Eqn 15, 17, 18). Accuracy in

estimating J_{ATP} is critical, especially for g_{BS} fitting, which is based on the additional J_{ATP} demand brought about by the PCO cycle under ambient O_2 (which, of course, is minimal as the C_4 CCM suppresses photorespiration). We propose three approaches to calculate J_{ATP} that can be selected depending on the particular modelling requirements.

Firstly, following the approach of Yin, sheets 8, 9, 10, and 12 calculate J_{ATP} as:

$$J_{ATP} = \frac{s'\, Y(II)\, PPFD}{1 - x} \qquad 8$$

Alternatively, following Valentini, sheets 8, 9, 10, and 12 calculate J_{ATP} as:

$$J_{ATP} = \frac{5}{k'}\,(Y(II) - b)\, PPFD \qquad 9$$

Where relevant quantities have been previously defined. Eqn 8 and 9 differ by the parameter b which is the fraction of Y(II) not used by C_4, RPP, and PCO cycles. The difference is negligible under limiting PPFD, but becomes appreciable under moderate or high PPFD. Eqns 8 and 9 are underpinned by three assumptions: 1) R_{LIGHT} does not vary with light level; 2) s′, k′ and b are constant, that is, the degree of engagement of alternative sinks and cyclic electron flow do not vary with PPFD or C_i; 3) ATP partitioning between C_4 and C_3 activity is constant. Deviations from linearity may arise from differential engagement of alternative sinks or experimental biases introduced by sub–saturating flash intensities (Harbinson, 2013), or also vertical differences in Y(II) quenching down the leaf profile (Bellasio et al., 2015, Evans, 2009). To account for non–linearity, we implemented the simple approach presented by Bellasio (Bellasio & Griffiths, 2014b). Sheets 8, 9, 10, and 12 calculate J_{ATP} for each point of the light and A/C_i curves as:

$$J_{ATP} = 5\, GA_{\mathrm{LOW}} \frac{Y(II)_{\mathrm{AMB}}}{Y(II)_{\mathrm{LOW}}}, \qquad 10$$

where $Y(II)_{AMB}$ and $Y(II)_{LOW}$ are the values of Y(II) measured under ambient and low O_2, respectively. 5 represents the ATP cost of GA under low O_2 (the value can be modified in the

EFT). Eqn 10 relies on assumption (1), it does not rely on assumption (2), and only partially relies on assumption (3), in the sense that the ATP partitioning between C_4 and C_3 activity is assumed constant only across O_2 levels but can vary between PPFD and C_i levels.

9. PPFD dependence of J_{ATP}

The process of photophosphorylation is driven by light and displays a saturating response to increasing PPFD which can be described empirically by a non–rectangular hyperbola (Farquhar & Wong, 1984) analogous to Eqn 2 and implemented in Sheet 9:

$$J_{\mathrm{ATPMOD\ Emp}} = \frac{Y(J_{\mathrm{ATP}})_{\mathrm{LL}}\, PPFD + J_{\mathrm{ATPSAT}} - \sqrt{(Y(J_{\mathrm{ATP}})_{\mathrm{LL}}\, PPFD + J_{\mathrm{ATPSAT}})^2 - 4\theta J_{\mathrm{ATPSAT}} Y(J_{\mathrm{ATP}})_{\mathrm{LL}}\, PPFD}}{2\theta}. \quad (11)$$

Eqn 11 describes the relationship between $J_{ATPMOD\ Emp}$ and PPFD in terms of J_{ATPSAT}, $Y(J_{ATP})_{LL}$, and θ. J_{ATPSAT} represents the value of J_{ATP} under infinite PPFD and defines the horizontal asymptote (J_{ATPMOD}=J_{ATPSAT}). $Y(J_{ATP})_{LL}$ represents the initial (and maximal) quantum yield for ATP production, defining the inclined asymptote (J_{ATPMOD}= $Y(J_{ATP})_{LL}$ PPFD). θ is an empirical factor ($0 \leq \theta \leq 1$) defining the curvature. To facilitate the physiological interpretation of θ, Sheet 9 calculates the PPFD which half saturates J_{ATPMOD} ($PPFD_{50}$) (analogous to $K_{1/2}$). With $Y(J_{ATP})_{LL}$ found in Step 7, J_{ATPSAT} and θ are derived in Sheet 9 by fitting J_{ATPMOD} (Eqn 12) to empirical values of J_{ATP} (Eqn 8, 9 or 10) calculated at each PPFD. This fitting is limited to ambient O_2, if J_{ATPMOD}, $Y(J_{ATP})_{LL}$, and J_{ATPSAT} are desired under low O_2, because of the assumption of non–photorespiratory conditions, they can be calculated from quantities derived in Sheet 4b as: $J_{ATPMOD} \approx 5\ GA_{MOD}$, $Y(J_{ATP})_{LL} \approx 5\ Y(CO_2)_{LL}$, $J_{ATPSAT} \approx 5\ GA_{SAT}$.

10. Bundle sheath conductance to CO_2 diffusion (g_{BS})

The C_4 (amino)acids diffuse through plasmodesmata from external M cells to an internal layer of cells, the BS, and are decarboxylated to supply CO_2 for Rubisco. For this CCM to work, the BS has to be partially isolated from the surrounding M, and the CO_2 permeability at the BS/M interface, known as the bundle sheath conductance to CO_2 (g_{BS}) has to be finely regulated (Bellasio & Griffiths, 2014b, Kromdijk et al., 2014). It is widely accepted that g_{BS} varies between different species and environmental conditions, however, resolving g_{BS} has challenged C_4 physiologists. For instance, g_{BS} has been resolved by fitting a 'modelled' isotopic discrimination to observed, on–line isotopic discrimination (Ubierna et al., 2011). Recent theoretical developments, coupled with refinements in gas exchange data analysis,

have allowed g_{BS} to be resolved from combined fluorescence–gas exchange datasets (Bellasio & Griffiths, 2014b, Yin et al., 2011b). With this approach, known as 'J/J', the C_4 photosynthesis model is rearranged (Ubierna et al., 2013) to express J_{ATPMOD} as:

$$J_{ATPMOD\ Mech.} = \frac{-y + \sqrt{y^2 - 4wz}}{2w}, \quad 12$$

where:

$w = \frac{x - x^2}{6A}$;

$y = \frac{1-x}{3}\left[\frac{g_{BS}}{A} + \left(C_M - \frac{R_M}{g_{BS}} - \gamma^* O_M\right) - 1 - \frac{\alpha\gamma^*}{0.047}\right] - \frac{x}{2}\left(1 + \frac{R_{LIGHT}}{A}\right)$;

$z = \left(1 + \frac{R_{LIGHT}}{A}\right)\left(R_M - g_{BS}\, C_M - \frac{7\, g_{BS}\, \gamma^* O_M}{3}\right) + (R_{LIGHT} + A)\left(1 - \frac{7\alpha\gamma^*}{3 \cdot 0.047}\right)$;

α is the fraction of PSII activity in BS cells; γ^* is half the reciprocal Rubisco CO_2/O_2 specificity; O_M is the oxygen concentration in M; R_M is the M fraction of R_{LIGHT} (generally 0.5 R_{LIGHT}), and other variables were previously defined (Table 1). g_{BS} is found by iterative fitting J_{ATPMOD} to experimental values of J_{ATP} (Eqn 8, 9, or 10) in the light–limited region of the light curve (as a variant, the EFT allows the user to include the light–limited region of the A/C_i curve).

11. PEPC kinetics – In vivo maximum carboxylation rate (V_{PMAX}) and in vivo effective Michaelis–Menten constant for CO_2 (K_P)

In conditions of high PPFD and low C_i, assimilation is limited by enzyme capacity (von Caemmerer, 2000). In particular, the initial part of the A/C_i curve is determined by PEPC activity and can be described with a Michaelis–Menten response [Eqn 4.26 in (von Caemmerer, 2000)] as:

$$GA = \frac{C_M\, V_{PMAX}}{C_M + K_P}, \quad 13$$

where C_M is the CO_2 concentration in M, V_{PMAX} is the PEPC CO_2 saturated rate, K_P is PEPC Michaelis–Menten for CO_2. Eqn 13 is a mathematical approximation of a quadratic equation [Eqn 4.21 in (von Caemmerer, 2000)]:

$$A_C = \frac{-p-\sqrt{q^2-4pr}}{2p},$$

where:

$$p = 1 - \frac{aK_C}{0.047K_O};$$

$$q = -\left[V_P - R_M + g_{BS}\,C_M + V_{CMAX} - R_{LIGHT} + g_{BS}K_C\left(1+\frac{O_M}{K_O}\right) + \frac{a}{0.047}\left(\gamma^* V_{CMAX} + R_{LIGHT}\frac{K_C}{K_O}\right)\right];$$

$$r = (V_{CMAX} - R_{LIGHT})(V_P - R_M + g_{BS}\,C_M) - V_{CMAX}\,g_{BS}\,\gamma^* O_M + R_{LIGHT}\,g_{BS}K_C\left(1+\frac{O_M}{K_O}\right);$$

0.047 is a coefficient scaling O_2 and CO_2 diffusivity (von Caemmerer, 2000); γ* is half the reciprocal Rubisco specificity and it is often taken from in vitro studies (e.g. 0.000193); C_M is calculated with Eqn 19, O_M is the O_2 concentration in M, generally assumed to equal the atmospheric O_2 concentration, V_{CMAX} is the Rubisco CO_2–saturated rate of carboxylation; K_C is the Rubisco Michaelis–Menten constant for CO_2; K_O is the Rubisco Michaelis–Menten constant for O_2; and other quantities were previously defined. In Sheet 11, Eqn 14 is fitted to the initial part of the A/C_i curve (limitation '1' and '2') to estimate V_{PMAX} and K_P in a single fitting step. Alternatively, if an in vitro value for K_P is used, only V_{PMAX} can be fitted. In Sheet 11b, Eqn 14 is fitted to the low O_2 A/C_i curve and, additionally, ambient and low O_2 A/C_i curves can be fitted concurrently (see instructions in Sheet 11b).

Although V_{CMAX}, K_C, and K_O appear in Eqn 14, they cannot be reliably estimated by curve fitting, and are preferably taken from in vitro studies. In fact, as seen above, under low C_i Eqn 14 is approximated by Eqn 13 whose behaviour is independent of V_{CMAX}, K_C, and K_O. Under higher C_i, CO_2 assimilation rate is no–longer enzyme–limited, and consequently cannot be modelled using enzyme kinetic equations (Eqn 13 and 14). Moreover, a very poor correlation with in vitro Rubisco CO_2 saturated carboxylation rate was found with attempts to estimate V_{CMAX} by fitting Eqn 14 to A/C_i data (Pinto et al., 2014).

12. PEP carboxylation rate (V_P), Rubisco rate of Carboxylation (V_C) and Oxygenation (V_O)

V_P, V_O, and V_C cannot be measured directly by gas exchange, but they can be estimated using the light–limited equations of the C_4 model (von Caemmerer, 2000). The fraction of J_{ATP} partitioned to PEP regeneration can be calculated through an assumed partitioning factor called x (see also Step 7). Knowing that PEP synthesis requires 2 ATP, V_P can be calculated as:

$$V_P = \frac{x\,J_{ATP}}{2}.$$

The complement (1-x)J_{ATP} represents the fraction of J_{ATP} partitioned to the RPP and PCO cycles. Knowing that each Rubisco carboxylase catalytic event requires 3 ATP, while each Rubisco oxygenase catalytic event requires 3.5 ATP, it can be written:

$$(1-x)\,J_{ATP} = 3V_c + 3.5V_O \qquad 16$$

Further, the leaf CO_2 balance can be formulated as:

$$GA = V_c - \frac{1}{2}V_O. \qquad 17$$

When Eqn 17 is substituted in Eqn 16, V_O can be solved as:

$$V_O = \frac{(1-x)\,J_{ATP} - 3GA}{5}. \qquad 18$$

The rate of photorespiratory CO_2 release can be calculated as F=½V_O and V_C can be solved from Eqn 16. J_{ATP} in Eqns 15–18 is calculated after Yin (Eqn 8), Valentini (Eqn 9) or Bellasio (Eqn 10). The Yin calibration is based on the initial light–limited portion of the light curves and is preferably used only in this narrow interval. The Valentini calibration is based on all light–limited datapoints, and should not be used outwith these. The Bellasio calibration can be used flexibly to calculate any datapoint. In fact, although Eqns 15–18 assume light (and ATP) limitations, they may be valid not only when ATP is actually limiting, but also when the ATP demand for PEP regeneration, RPP, and PCO cycles fully feedback to the electron transport chain. This condition is generally satisfied, as thylakoid reactions are tightly regulated by ATP and NADPH demand (Kramer & Evans, 2011), although, the regulation of thylakoid reactions may differ under different limitations (see Discussion). For this reason, although Sheet 12 calculates Eqns 15–18 for all datapoints, enzyme–limited datapoints are highlighted in red and results should be taken with care. Values can be compared with the enzyme–limited formulation in additional features in Sheet 12.

13. CO_2 concentration in M (C_M), CO_2 and O_2 concentration in BS (C_{BS} and O_{BS}), Leak rate (L), and bundle sheath leakiness (ϕ)

The process of CO_2 diffusion in C_4 parenchyma consists of several steps. Starting from the intercellular air spaces, CO_2 diffuses into the liquid phase through the cell walls, the plasmalemma, and the cytosol, where CO_2 is hydrated to HCO_3^-, the substrate of PEPC. The overall ability to conduct CO_2 through this path is mathematically expressed as the mesophyll conductance (g_M) and the CO_2 concentration in M can be expressed as:

$$C_M = C_i - \frac{A}{g_M}. \quad 19$$

Because the C_4 diffusion path is shorter than that for C_3 plants, C_4 g_M is larger than C_3 g_M. However, C_4 g_M values are still subject to debate [because of numerous experimental limitations, see (Ubierna et al., 2011) for review].

CO_2 is more concentrated in BS than M (see Step 10 above), and because BS and M are connected by plasmodesmata, some CO_2 retrodiffuses. This 'leakage' is an inherent process of the CCM. The rate of CO_2 retrodiffusion is called leak rate (L), and the law of diffusion can be written as:

$$C_{BS} = C_M + \frac{L}{g_{BS}}. \quad 20$$

Of the quantities in Eqn 20, g_{BS} was derived by curve fitting in Step 10 while C_{BS} and L are yet to be determined. A first approach to resolve C_{BS} and L, which we call 'mass balance' determines L from M mass balance as:

$$L = V_P - R_M - A \quad 21$$

Eqn 21 can be solved with V_P (calculated with Eqn 15), measured A, and R_{LIGHT} (the fraction R_M/R_{LIGHT} is generally assumed, Table 1). C_{BS} can then solved from Eqn 20.

A second approach, which we call 'Rubisco specificity', estimates C_{BS} from the Rubisco oxygenation vs carboxylation ratio (V_O/V_C, Eqn 16 and 18), given a certain Rubisco specificity and O_2 concentration in BS, or in the equivalent notation of (von Caemmerer, 2000):

$$C_{\mathrm{BS}} = \frac{(\gamma^* O_{BS})\left[\frac{7}{3}GA + \frac{(1-x)J_{ATP}}{3}\right]}{\frac{(1-x)J_{ATP}}{3} - GA}, \quad 22$$

where O_{BS}, the O_2 concentration in BS, is calculated as:

$$O_{\mathrm{BS}} = \frac{\alpha A}{0.047 g_{\mathrm{BS}}} + O_{\mathrm{M}}, \quad 23$$

where terms are defined in Table 1. Finally, L can be solved from Eqn 20 using g_{BS} derived in Step 10. Note that the logic and parameter requirements of the mass balance and Rubisco specificity approaches are different. The mass balance approach depends on J_{ATP} and x, whereas the Rubisco specificity approach is mathematically independent of J_{ATP} and x if consistency is maintained between Eqn 8, 9, or 10 and Eqn 16 and 18 (see also Discussion).

A useful term in C_4 physiology is leakiness (ϕ), defined as the leak rate relative to the PEP carboxylation rate ($\phi = L/V_P$). Since Rubisco CO_2 fixation (in BS) is complementary to leakage (out of BS), ϕ can be used as a proxy for the coordination between the CCM and C_3 assimilatory activity. Further, under conditions of non–limiting light, when leaking CO_2 is entirely re–fixed by PEPC, ϕ can be used as a proxy of biochemical operating efficiency [see exceptions and references in (Bellasio & Griffiths, 2014a)]. Leakiness is believed to be tightly regulated to optimise C_4 operating efficiency (Bellasio & Griffiths, 2014b, Kromdijk et al., 2014). The EFT calculates ϕ with both the mass balance (Eqn 13, 18, and 19) and Rubisco specificity (Eqn 18, 20, and 21) approaches.

Applying the EFT to primary data from Zea mays L.: a worked example

Genetically identical maize plants (F1 Hybrid PR31N27, Pioneer Hi–bred, Cremona, Italy) were grown in controlled environment growth rooms (BDW 40 Conviron Ltd, Winnipeg, Canada) set at 14h day length, PPFD = 350 μmol m^{-2} s^{-1}, temperature of 27 °C / 18 °C, and 50% / 70 % relative humidity (day / night). Plants were manually watered daily, with particular care to avoid overwatering. The apical part of the youngest fully expanded leaf was subject to combined gas exchange and fluorescence analysis.

A portable gas exchange system (GES, LI6400XT, LI–Cor, USA), was factory–modified to control at low CO_2 concentrations (a webinar is available on the LI–COR website). The GES was fitted with a 6 cm^2 'sun+sky' cuvette, upper and lower black neoprene gaskets, and with a LI–COR 6400–18 RGB light source, positioned to uniformly illuminate the leaf. The

aluminium casing of the cuvette was perforated to fit the light sensor removed from the RGB light source, which was calibrated using a factory–calibrated Li–250 light sensor (LI–Cor, USA) according to the manufacturer's instructions (Doug Lynch, personal communication), and a fibre probe (⌀ 1.5 mm) fitted at 45° and c. 1mm distance from the leaf. The fibre probe was connected to a Junior PAM (Heinz Walz GmbH, Effeltrich, D). Pulse width was set to 0.4 s, pulse intensity was set to level 9, enough to saturate P signal (which occurred between level 6 and 8). Mass flow leaks (Boesgaard et al., 2013) were monitored with a gas flow meter as detailed in (Bellasio et al., 2015), but no sealant was necessary. A R_{DARK}/C_a response curve was measured by setting reference CO_2 at 0, 400, 800 and 1200 μmol mol^{-1}, flow set at 400 mmol min^{-1}. After stabilising at each level, the GES was matched and assimilation was measured every 5s for c. 60s (and then averaged). A diffusion correction term 'k' (Walker & Ort, 2015) and R_{DARK} were determined by linear curve fit, taking 400 μmol mol^{-1} as the lab CO_2 concentration (an example is provided in Supporting Information).

Light was set at a PPFD of 30 μmol m^{-2} s^{-1}; after 10 min acclimation the GES was matched and assimilation was measured every 5s for c. 60s (and then averaged), and a saturating pulse was applied to determine Y(II). The background gas was switched to 2% O_2, after six minutes, measurements were taken again. The background gas was switched to air and the routine was repeated to measure at PPFD of 50, 75, 100, 150, 300, 600 and 1200 μmol m^{-2} s^{-1}. Flow was set at 150 mmol min^{-1} (first 5 points) and then increased to 400 mmol min^{-1} for the rest of the measurements (Bellasio et al., 2015). The A/C_i curves were measured at PPFD level of 1200 μmol m^{-2} s^{-1}. Reference CO_2 was set at 500 μmol mol^{-1} and the background gas was switched to air, after six minutes' acclimation the GES was matched and assimilation was measured every 5s for c. 30s (and then averaged) and a saturating pulse was applied to determine Y(II). The background gas was switched to 2% O_2, after six minutes' acclimation the GES was matched and measurements were taken again. The routine was repeated to measure at a reference CO_2 of 400, 300, 200, 100, 60, 40, 20, 10 μmol m^{-2} s^{-1}. Upon switching background gas, the O_2 concentration was specified in the GES software. This protocol took c. 8h, and was repeated on n=3 plants. Experimental practicalities are discussed in Discussion.

Primary data were corrected for CO_2 diffusion through the gaskets as:

$$A = Photo + \frac{k\,(400 - C_a)}{100\,Area}, \qquad 21$$

where Photo is the uncorrected assimilation as calculated by the LI–COR software, 400 is the CO_2 concentration outside the cuvette, C_a is the CO_2 concentration in the cuvette (CO2S in the LI–COR notation) and Area is the leaf area (6 cm^2 in this example), k was derived by linear fit as detailed above. C_i was recalculated using the LI–COR equations inputting A calculated with Eqn 21. Diffusion–corrected data are shown in Figure 1.

Because of the low O_2 susceptibility of C_4 physiology, differences in net assimilation between ambient and low O_2 were small but consistent (c. 0.3 μmol m^{-2} s^{-1}) for both the light and A/C_i curves. Y(II) was lower under low O_2 (dotted line) reflecting the smaller ATP demand under non–photorespiratory conditions. Data were analysed using the 13–step approach of the EFT, summarised below.

1. Thresholds used to assign datapoints were, for light–curves: '1' PPFD < 300 μmol m^{-2} s^{-1}; '2' remainder of datapoints. For A/C_i curves: '1' $C_i \leq 20$ μmol mol^{-1}; '2' $20 < C_i < 40$ μmol mol^{-1}; '2.5' $40 < C_i < 70$ μmol mol^{-1} (these datapoints were excluded from V_{PMAX} fitting, Step 11), and '3' $C_i > 70$ μmol mol^{-1}.

2. R_{LIGHT} was derived under ambient and low O_2 using linear regressions (Eqn 1).

3. $Y(II)_{LL}$ was derived with linear regression.

4. GA was calculated under ambient and low O_2 using the values of R_{LIGHT} derived in Step 2. The PPFD dependence of GA was modelled to derive GA_{SAT}, $PPFD_{50}$, and $Y(CO_2)_{LL}$. Residuals were log–transformed to correct for proportionality between residuals and GA, thus providing a better fit in the initial (low PPFD) region of the curve. The LCP was slightly higher under ambient O_2 reflecting the additional light requirements for operating the PCO cycle. GA_{SAT} was slightly higher under low O_2 because of the additional ATP and NADPH availability for CO_2 assimilation. $Y(CO_2)_{LL}$ was slightly higher under low O_2 reflecting the higher conversion efficiency of light into fixed CO_2.

5. The C_i dependence of A was modelled under ambient and low O_2 to derive CE, A_{SAT}, C_{i50}, and Γ. Residuals were log–transformed to improve fit in the initial (low C_i) region of the curve. Parameters reflect a low O_2 susceptibility, however L_S was slightly higher under low O_2.

6a. The Yin calibration was performed with standard settings.

6b. The Valentini calibration was performed using R_{LIGHT} estimated in Step 2 under low O_2, and limiting the regression to light–limited datapoints taken from the light curve (limitation '1' and '2') and A/C_i curve (limitation '3'). The fit was good R^2 c. 0.99, but in this case the calibration is valid only for light–limited datapoints. The parameter, b, which is responsible

for differences between the Valentini and Yin J_{ATP} derivation (see 9), was substantially different from 0.

7. $Y(J_{ATP})_{LL}$ was unaffected by the O_2 level, as expected.

8. J_{ATP} was calculated using the Valentini calibration. Values are shown in Figure 2A (light curves) and 2B (A/C_i curves) only for light–limited datapoints. If values for J_{ATP} are desired for other datapoints the calibration of Bellasio can be used instead (but see Discussion).

9. The PPFD response of J_{ATP} was modelled to derive J_{ATPSAT} , θ, and $PPFD_{50}$.

10. g_{BS} was estimated by fitting data pooled from the light and A/C_i curves (only the three points at the highest C_i), using R_{LIGHT} derived under ambient O_2 in Sheet 2 and J_{ATP} shown in Figure 2A and 2B. Assumed values for O_M, α, g_M, m, γ*, and x are listed in Table 1. R_M/R_{LIGHT} was assumed to be 0.5. Residuals were log–transformed to correct for proportionality between residuals and J_{ATP}.

11. V_{PMAX} was estimated using R_{LIGHT} derived in Step 2 and g_{BS} derived in Step 10, by curve fitting to the enzyme–limited region of the A/C_i curve (limitations '1' and '2'). Assumed values for O_M, α, g_M, γ*, x, and Rubisco kinetic constants K_C, K_O, and V_{CMAX} are listed in Table 1. R_M/R_{LIGHT} was assumed to be 0.5. Although K_P could be fitted concurrently to V_{PMAX}, in this example it was assumed to be 80 μbar (von Caemmerer, 2000) to increase constraint.

12. The rates of Rubisco carboxylation, oxygenation, and photorespiratory CO_2 release were calculated for each datapoint, using J_{ATP} values shown in Figure 2A and 2B. V_O/V_C ratios are shown in Figure 2C (light curve) and 2D (A/C_i curve).

13. CO_2 concentration in M, BS, CO_2 leak rate and leakiness were calculated with the mass balance approach, using g_{BS} derived in Step 10 and the values of J_{ATP} derived in Step 8 with the Valentini calibration. Assumed values for O_M, α, g_M, γ*, x, are listed in Table 1. R_M/R_{LIGHT} was assumed 0.5.Figure 2E and G (light curve) and 2F and H (A/C_i curve) shows the calculated values for C_{BS} and leakiness (ϕ) respectively. These display the expected trend at low light intensity and are within the physiological limits for the light–limited points of A/C_i curve.

Discussion

We have developed a tool for the analysis of gas exchange data embedded with a model of C_4 photosynthesis. The key output from the data analysis is the ATP production rate J_{ATP}, which is inputted to the C_4 model to derive detailed information on C_4 photosynthesis such as V_P, C_{BS} and L. Because these approaches are integrated, some uncertainties of model

parameterisation are avoided. Further, the step–by–step logic allows inputs based on various independent model sources to be compared, and model fitting to the data is straightforward and easily modified. Some sources of error associated with model assumptions or uncertain parameterisation, however, remain. These are now briefly reviewed, together with sources of experimental error which, although not strictly related to data analyses, could affect the quality of results.

Experimental sources of error.

Because C_4 photosynthesis suppresses photorespiration, the difference in photosynthetic rates between ambient and low O_2 are minimal (as low as 1%), and so are the difference between $Y(II)_{LOW}$ and $Y(II)_{AMB}$. These differences are used to calculate J_{ATP} and are translated into V_O/V_C, which, in C_4 plants is as low as 3–5%. Distinguishing these small differences is an experimental challenge, hence high quality data, in terms of precision and accuracy, are essential [for theory of error see (Bellasio et al., 2014b) and references therein]. We briefly mention the important experimental practicalities of gas exchange measurements, for details see Supporting Information in Bellasio et al. (2015). CO_2 diffusion through the gaskets is a well–known source of error of GES (Flexas et al., 2007) which becomes substantial when the experiment is undertaken using small chambers (Pons et al., 2009). As compared to the tobacco example in Bellasio et al. (2015), where a 2 cm^2 chamber was used, here we preferred a 6 cm^2 chamber, with two black neoprene gaskets. It was recently pointed out that mass–flow leaks resulting from a poor seal between the gasket and the leaf alter diffusion (Boesgaard et al., 2013). Mass flow leaks were monitored with a flowmeter as detailed in Bellasio et al. (2015) and for these measurements it was not necessary to apply additional sealant around the main vein. To correctly account for diffusion we derived a measurement–specific coefficient of diffusion 'k' by linear regression (example provided in Supporting Information) of R_{DARK}/C_a curves (Walker & Ort, 2015). In agreement with Walker and Ort (2015) we found that the mean k did not differ from the suggested value of 0.4, however we noted some variability so there may be scope for calibrating each replicate leaf.

It is well–known that sub–saturating light pulses will artificially lower Y(II) (Earl & Ennahli, 2004). This issue arises particularly when using whole–chamber fluorometers, which generally have a lower saturating pulse intensity than fibre probe fluorometers. Although the method proposed here recalibrates the relationship between Y(II) and J_{ATP} for each individual plant, and therefore minimises any effect of systematic error, we used a fluorometer working on a small fibre probe. We found this solution very reliable, particularly for the possibility of reaching the vicinity of the leaf without shading and regulating the

saturating pulse intensity (which was determined in a pilot experiment) so as to saturate the P signal (Harbinson, 2013, Loriaux et al., 2013).

Light intensity levels were chosen bearing in mind that high resolution between 30 and 150 μmol m^{-2} s^{-1} is required when obtaining light–curves for fitting respiration in the light (R_{LIGHT}) and to calibrate s′ according to Yin, while relatively fewer points are required at high PPFD to fit the light–saturated rate of ATP production $J_{ATP\ SAT}$. Here we preferred not to use saturating PPFDs so that the points at high PPFD could be used in the fitting of g_{BS}, which works under the assumption of light–limitation. Similarly, the light intensity under which A/C_i curves were measured was intermediate so that datapoints obtained under ambient C_a were light–limited and used for g_{BS} fitting. To provide a sufficient number of datapoints under low C_i to fit $V_{P\ MAX}$ we had the GES factory–modified to reach very low CO_2 concentrations. With this particular experimental routine, when the enzyme–limited datapoints were plotted for the Valentini calibration, they had a different slope and intercept than the light–limited datapoints. This behaviour is generally attributed to the existence of alternative electron sinks. Here it may be due to: a difference in regulation of PSII under light–limitation, rather than under enzyme–limitation; to a changing profile of PSII quenching through the thickness of the leaf (Evans, 2009, Kaiser et al., 2014); or because BS and M are spatially separated to a different partitioning of thylakoid reactions between BS and M. These considerations are beyond the scope of this review and we refer the reader to specialised literature (Bellasio & Griffiths, 2014c, Kramer & Evans, 2011, Yin & Struik, 2012). To avoid any issue of non–linearity we limited the application of the light–limited model to light–limited datapoints in the Valentini calibration (Sheet 6b), in the derivation of g_{BS} (Sheet 10) and in the subsequent parameterisation of the C_4 model (Sheet 12–13). It has been noted, however, that light–limited equations may be applied beyond the strictly light–limited datapoints (Archontoulis et al., 2012). For this reason the model output was calculated for all datapoints regardless of the limitation. Further, we included the Bellasio calibration, which is point–to–point based and can be used more flexibly than the Valentini or Yin calibrations, and we also included the enzyme–limited formulation in additional features of Sheet 12–13 in order to provide a useful comparison. Because of these technical difficulties it may be productive to concentrate on a smaller dataset, and opt for data quality over quantity (see also Partial datasets, below). For instance, the light–limited part of the light curve is ideal to estimate g_{BS} (Bellasio & Griffiths, 2014b), while the enzyme–limited part of the A/C_i curve can highlight any effect on PEPC activity (Pinto et al., 2014).

Finally, the O_2 concentration in the background gas modifies the infra–red absorption of H_2O (Bunce, 2002), and will affect the estimate for $[H_2O]$, and hence transpiration, g_S and C_i. LI–COR, for example, has built the ability to specify gas mixtures different from air into the

GES software (see LI–COR manual for details). If this correction cannot be implemented (e.g. reanalysing an existing dataset or working with a different GES), the EFT can still be used, avoiding sheets 5b, and 11b, which rely on [H_2O] measured under low O_2. All other sheets are valid, as based on [CO_2] and [H_2O] measured under ambient O_2, and on [CO_2] measured under low O_2.

Validity and Applicability

The EFT developed previously by Bellasio et al. (2015) is based on NADPH–limited equations, which are valid for any photosynthetic type, but do not allow for V_P, C_{BS} and L to be derived. Here we developed the ATP–limited equations, which allow such derivations, but necessitate assumption of the ATP cost of gross assimilation under low O_2, $\frac{ATP}{GA}_{LOW}$, and the value of a partitioning factor called x, which specifies the fraction of ATP consumed by PEP regeneration. These assumptions introduce uncertainty. We will now distinguish two cases, when $\frac{ATP}{GA}_{LOW}$ and x are known with a reasonable degree of confidence, and when $\frac{ATP}{GA}_{LOW}$ and x are unknown. First is the case of C_4 photosynthesis where x was predicted to have limited variability across a range of conditions (Kromdijk et al., 2010, von Caemmerer, 2000). $\frac{ATP}{GA}_{LOW}$ was proposed to be determined by x as $\frac{ATP}{GA}_{LOW} = \frac{3}{1-x}$ (Tazoe et al., 2008, von Caemmerer, 2000, Yin et al., 2011b), i.e. $\frac{ATP}{GA}_{LOW} \approx 5$. There are assumptions within this equation that need to be carefully considered: 1) respiratory ATP and NADPH are assumed to be entirely consumed by basal metabolism; 2) respiration is assumed to be supplied by old assimilates (Stutz et al., 2014), thus respiratory PGA consumption is neglected; 3) PEP carboxykinase (PEPCK) activity is neglected; 4) starch synthesis and sucrose loading have no ATP cost. A metabolic model can be used to study the influence of each of these variables on $\frac{ATP}{GA}_{LOW}$, and a freely available version is provided in the supporting information of McQualter et al. (2015). Because PEPCK catalytic cycle requires half the ATP of PPDK, a moderate PEPCK can compensate for the ATP cost of carbohydrate synthesis, resulting in $\frac{ATP}{GA}_{LOW} \approx 5$. Complete PEPCK engagement would result in $\frac{ATP}{GA}_{LOW} < 5$, but as the PEPCK reaction may not be fast enough to sustain high decarboxylation rates, such a situation is unlikely. In these conditions part of the newly synthesized PEP may be necessarily hydrolysed to drive the PEPCK reaction (Richard Leegood, personal communication), allowing $\frac{ATP}{GA}_{LOW} \approx 5$. Even within these confidence limits the C_4 model would be highly sensitive to any uncertainty in $\frac{ATP}{GA}_{LOW}$ and x, but the error would be small relative to the

experimental error discussed above. The application to C_3 photosynthesis, which emerges as a special case when x=0 and $\frac{ATP}{GA}_{LOW} = 3$, would also be well constrained. In this condition the EFT would code the ATP–limited model of C_3 photosynthesis. Sheets 1–10 and 11–12 would also be valid, and can be inputted x=0 and $\frac{ATP}{GA}_{LOW} = 3$ (Sheets, cells: 6a, T15; 6b, U13; 8–9, H3; 10, J8; 12–13, Q4). Sheet 10 would be operating similarly to the derivation of C_3 g_M, but based on ATP requirements, while the derivation of V_{PMAX} would be invalid.

Secondly, when $\frac{ATP}{GA}_{LOW}$ and x are not known, the EFT can still be used, but different steps need to be taken. This scenario could allow disrupted C_4 photosynthesis to be studied, with variable PEPC engagement, and Rubisco entirely located in BS. In this case J_{ATP} (Eqn 8, 9 and 10), V_P (Eqn 15), and the mass balance approach to estimate C_{BS} would not be resolved. Because similar multipliers are used when calculating Eqn 8, 9 or 10 and Eqn 16 and 18, V_O/V_C, are mathematically independent of the value of $\frac{ATP}{GA}_{LOW}$ and x, as long as they satisfy $\frac{ATP}{GA}_{LOW} = \frac{3}{1-x}$. Test values for $\frac{ATP}{GA}_{LOW}$ and x could be entered in the aforementioned cells, C_{BS} could then be determined from V_O/V_C with the Rubisco specificity approach, and then used to calculate L through Eqn 20 and V_P through Eqn 21. Using this reverse logic x and $\frac{ATP}{GA}$ in a dysfunctional C_4 plant could, in principle, be estimated. Alternatively, V_O/V_C could be determined with the NADPH–limited equations in the previous EFT (Bellasio et al., 2015) and then follow the same logic ($V_O/V_C \rightarrow C_{BS} \rightarrow L \rightarrow V_P$). This model cannot be used when Rubisco activity is shared between BS and M, which requires the intermediate model of C_3–C_4 assimilation (von Caemmerer, 2000).

Adjusting for temperature and pressure

Consistency between the temperature of validity for input parameters (e.g. γ^*, g_M, V_{CMAX}, K_C) and the temperature at which the response curves are measured is essential. Parameters can be temperature–adjusted using exponential equations (Bernacchi et al., 2003, Bernacchi et al., 2002, Bernacchi et al., 2001, June et al., 2004, Scafaro et al., 2011, Yamori & von Caemmerer, 2009). Because empirical constants for temperature adjustment are available for only a limited number of parameters and species, they could not be implemented as a general tool in the EFT.

The EFT was developed to allow (diffusion corrected) gas exchange data to be inputted directly, whereby CO_2 levels are normally expressed as concentration (μmol mol^{-1}). This way of expressing CO_2 is convenient as it is independent of pressure, however, it is a simplification valid only at the pressure of 10^5 Pa. In fact, enzyme reaction rates depend on

the chemical activity of CO_2 expressed as fugacity. When CO_2 behaves as an ideal gas, fugacity is proportional to the partial pressure of the gas in equilibrium with the air above the liquid, in conditions outwith these limits fugacity should be used instead of concentration (Sharkey et al., 2007).

Use of the EFT with partial datasets

It is still possible to use the EFT when only a limited number of datapoints is available, however, it is recommended that the minimum requirements listed in Table 2 are met, and to ensure that all datapoints and parameters used in the calculations are available. To ensure the maximum flexibility of the EFT, all automatically populated data, placed in cells with a light background, can be manually overwritten.

Conclusion

Using combined fluorescence–A/C_i and fluorescence–light–response curves, measured under ambient and low O_2, the Excel–based fitting tool (EFT) can be used to derive a comprehensive suite of C_4 physiological parameters. These are derived with a step–by–step logic to avoid many of the uncertainties associated with concurrent multi–model applications. All steps are implemented in a freely downloadable Excel workbook that can be modified easily by the user. The parameters derived by the EFT summarise the physiological traits of the plant(s) measured and can be used to compare different plants or to parameterise predictive models. Overall, the EFT integrates the latest developments in the theory of gas exchange, fluorescence and C_4 modelling.

Acknowledgments

We are grateful to Joe Quirk and Marjorie Lundgren for critical review. We gratefully acknowledge funding of CB through an ERC advanced grant (CDREG, 322998) awarded to DJB.

The Authors have no conflict of interest.

References

Archontoulis S.V., Yin X., Vos J., Danalatos N.G. & Struik P.C. (2012) Leaf photosynthesis and respiration of three bioenergy crops in relation to temperature and leaf nitrogen: how conserved are biochemical model parameters among crop species? *Journal of Experimental Botany*, **63**, 895-911.

Bellasio C., Beerling D.J. & Griffiths H. (2015) An Excel tool for deriving key photosynthetic parameters from combined gas exchange and chlorophyll fluorescence: theory and practice. *Plant Cell and Environment*, **DOI: 10.1111/pce.12560**.

Bellasio C., Burgess S.J., Griffiths H. & Hibberd J.M. (2014a) A high throughput gas exchange screen for determining rates of photorespiration or regulation of C4 activity. *Journal of Experimental Botany*, **65**, 3769-3779.

Bellasio C., Fini A. & Ferrini F. (2014b) Evaluation of a High Throughput Starch Analysis Optimised for Wood. *PLoS ONE*, **9**, e86645.

Bellasio C. & Griffiths H. (2014a) Acclimation of C4 metabolism to low light in mature maize leaves could limit energetic losses during progressive shading in a crop canopy. *Journal of Experimental Botany*, **65**, 3725-3736.

Bellasio C. & Griffiths H. (2014b) Acclimation to Low Light by C4 maize: Implications for Bundle Sheath Leakiness. *Plant Cell and Environment*, **37**, 1046-1058.

Bellasio C. & Griffiths H. (2014c) The operation of two decarboxylases (NADPME and PEPCK), transamination and partitioning of C4 metabolic processes between mesophyll and bundle sheath cells allows light capture to be balanced for the maize C4 pathway. *Plant Physiology*, **164**, 466-480.

Bernacchi C.J., Pimentel C. & Long S.P. (2003) In vivo temperature response functions of parameters required to model RuBP-limited photosynthesis. *Plant, Cell & Environment*, **26**, 1419-1430.

Bernacchi C.J., Portis A.R., Nakano H., von Caemmerer S. & Long S.P. (2002) Temperature Response of Mesophyll Conductance. Implications for the Determination of Rubisco Enzyme Kinetics and for Limitations to Photosynthesis in Vivo. *Plant Physiology*, **130**, 1992-1998.

Bernacchi C.J., Singsaas E.L., Pimentel C., Portis Jr A.R. & Long S.P. (2001) Improved temperature response functions for models of Rubisco-limited photosynthesis. *Plant, Cell & Environment*, **24**, 253-259.

Boesgaard K.S., Mikkelsen T.N., Ro-Poulsen H. & Ibrom A. (2013) Reduction of molecular gas diffusion through gaskets in leaf gas exchange cuvettes by leaf-mediated pores. *Plant, Cell & Environment*, **36**, 1352-1362.

Brooks A. & Farquhar G.D. (1985) Effect of temperature on the CO2/O2 specificity of ribulose-1,5-bisphosphate carboxylase/oxygenase and the rate of respiration in the light. *Planta*, **165**, 397-406.

Bunce J. (2002) Sensitivity of infrared water vapor analyzers to oxygen concentration and errors in stomatal conductance. *Photosynthesis Research*, **71**, 273-276.

Cernusak L.A., Ubierna N., Winter K., Holtum J.A.M., Marshall J.D. & Farquhar G.D. (2013) Environmental and physiological determinants of carbon isotope discrimination in terrestrial plants. *New Phytologist*, **200**, 950-965.

Earl H. & Ennahli S. (2004) Estimating photosynthetic electron transport via chlorophyll fluorometry without Photosystem II light saturation. *Photosynthesis Research*, **82**, 177-186.

Evans J.R. (2009) Potential Errors in Electron Transport Rates Calculated from Chlorophyll Fluorescence as Revealed by a Multilayer Leaf Model. *Plant and Cell Physiology*, **50**, 698-706.

Farquhar G.D. & Sharkey T.D. (1982) Stomatal Conductance and Photosynthesis. *Annual Review of Plant Physiology and Plant Molecular Biology*, **33**, 317-345.

Farquhar G.D. & Wong S.C. (1984) An Empirical-Model of Stomatal Conductance. *Australian Journal of Plant Physiology*, **11**, 191-209.

Flexas J., Diaz-Espejo A., Berry J.A., Cifre J., Galmes J., Kaidenhoff R., . . . Ribas-Carbo M. (2007) Analysis of leakage in IRGA's leaf chambers of open gas exchange systems: quantification and its effects in photosynthesis parameterization. *Journal of Experimental Botany*, **58**, 1533-1543.

Genty B., Briantais J.M. & Baker N.R. (1989) The relationship between the quantum yield of photosynthetic electron-transport and quenching of chlorophyll fluorescence. *Biochimica Et Biophysica Acta*, **990**, 87-92.

Harbinson J. (2013) Improving the accuracy of chlorophyll fluorescence measurements. *Plant, Cell & Environment*, **36**, 1751-1754.

Hibberd J.M., Sheehy J.E. & Langdale J.A. (2008) Using C4 photosynthesis to increase the yield of rice—rationale and feasibility. *Current Opinion in Plant Biology*, **11**, 228-231.

June T., Evans J.R. & Farquhar G.D. (2004) A simple new equation for the reversible temperature dependence of photosynthetic electron transport: a study on soybean leaf. *Functional Plant Biology*, **31**, 275-283.

Kaiser E., Morales A., Harbinson J., Kromdijk J., Heuvelink E. & Marcelis L.F.M. (2014) Dynamic photosynthesis in different environmental conditions. *Journal of Experimental Botany*.

Kramer D.M. & Evans J.R. (2011) The Importance of Energy Balance in Improving Photosynthetic Productivity. *Plant Physiology*, **155**, 70-78.

Kromdijk J., Griffiths H. & Schepers H.E. (2010) Can the progressive increase of C4 bundle sheath leakiness at low PFD be explained by incomplete suppression of photorespiration? *Plant Cell and Environment*, **33**, 1935-1948.

Kromdijk J., Ubierna N., Cousins A.B. & Griffiths H. (2014) Bundle-sheath leakiness in C4 photosynthesis: a careful balancing act between CO2 concentration and assimilation. *Journal of Experimental Botany*, **65**, 3443-3457.

Long S.P. & Bernacchi C.J. (2003) Gas exchange measurements, what can they tell us about the underlying limitations to photosynthesis? Procedures and sources of error. *Journal of Experimental Botany*, **54**, 2393-2401.

Long Stephen P., Marshall-Colon A. & Zhu X.-G. (2015) Meeting the Global Food Demand of the Future by Engineering Crop Photosynthesis and Yield Potential. *Cell*, **161**, 56-66.

Loriaux S.D., Avenson T.J., Welles J.M., McDermitt D.K., Eckles R.D., Riensche B. & Genty B. (2013) Closing in on maximum yield of chlorophyll fluorescence using a single multiphase flash of sub-saturating intensity. *Plant, Cell & Environment*, **36**, 1755-1770.

Maroco J.P., Ku M.S.B., Lea P.J., Dever L.V., Leegood R.C., Furbank R.T. & Edwards G.E. (1998) Oxygen requirement and inhibition of C-4 photosynthesis - An analysis of C-4 plants deficient in the C-3 and C-4 cycles. *Plant Physiology*, **116**, 823-832.

McQualter R.B., Bellasio C., Gebbie L., Petrasovits L.A., Palfreyman R., Hodson M., . . . Nielsen L. (2015) Systems biology and metabolic modelling unveils limitations to polyhydroxybutyrate accumulation in sugarcane leaves; lessons for C4 engineering. *Plant Biotechnology Journal*, **DOI: 10.1111/pbi.12399**.

Osborne C.P. & Beerling D.J. (2006) Nature's green revolution: the remarkable evolutionary rise of C-4 plants. *Philosophical Transactions of the Royal Society B-Biological Sciences*, **361**, 173-194.

Pinto H., Sharwood R.E., Tissue D.T. & Ghannoum O. (2014) Photosynthesis of C3, C3–C4, and C4 grasses at glacial CO2. *Journal of Experimental Botany*, **65**, 3669-3681.
Pons T.L., Flexas J., von Caemmerer S., Evans J.R., Genty B., Ribas-Carbo M. & Brugnoli E. (2009) Estimating mesophyll conductance to CO2: methodology, potential errors, and recommendations. *Journal of Experimental Botany*, **60**, 2217-2234.
Sage R.F. & Stata M. (2015) Photosynthetic diversity meets biodiversity: The C4 plant example. *Journal of Plant Physiology*, **172**, 104-119.
Scafaro A.P., Von Caemmerer S., Evans J.R. & Atwell B.J. (2011) Temperature response of mesophyll conductance in cultivated and wild Oryza species with contrasting mesophyll cell wall thickness. *Plant, Cell & Environment*, **34**, 1999-2008.
Sharkey T.D., Bernacchi C.J., Farquhar G.D. & Singsaas E.L. (2007) Fitting photosynthetic carbon dioxide response curves for C3 leaves. *Plant Cell and Environment*, **30**, 1035-1040.
Singh J., Pandey P., James D., Chandrasekhar K., Achary V.M.M., Kaul T., . . . Reddy M.K. (2014) Enhancing C3 photosynthesis: an outlook on feasible interventions for crop improvement. *Plant Biotechnology Journal*, **12**, 1217-1230.
Stutz S.S., Edwards G.E. & Cousins A.B. (2014) Single-cell C4 photosynthesis: efficiency and acclimation of Bienertia sinuspersici to growth under low light. *New Phytologist*, **202**, 220-232.
Tazoe Y., Hanba Y.T., Furumoto T., Noguchi K. & Terashima I. (2008) Relationships between quantum yield for CO2 assimilation, activity of key enzymes and CO2 leakiness in Amaranthus cruentus, a C4 dicot, grown in high or low light. *Plant and Cell Physiology*, **49**, 19-29.
Ubierna N., Sun W. & Cousins A.B. (2011) The efficiency of C4 photosynthesis under low light conditions: assumptions and calculations with CO2 isotope discrimination. *Journal of Experimental Botany*, **62**, 3119-3134.
Ubierna N., Sun W., Kramer D.M. & Cousins A.B. (2013) The Efficiency Of C4 Photosynthesis Under Low Light Conditions In Zea mays, Miscanthus X giganteus And Flaveria bidentis. *Plant, Cell & Environment*, **36**, 365-381.
Valentini R., Epron D., De Angelis P., Matteucci G. & Dreyer E. (1995) In situ estimation of net CO2 assimilation, photosynthetic electron flow and photorespiration in Turkey oak (Q. cerris L.) leaves: diurnal cycles under different levels of water supply. *Plant, Cell & Environment*, **18**, 631-640.
von Caemmerer S. (2000) *Biochemical models of leaf Photosynthesis*. CSIRO Publishing, Collingwood.
von Caemmerer S. & Farquhar G.D. (1981) Some Relationships between the Biochemistry of Photosynthesis and the Gas-Exchange of Leaves. *Planta*, **153**, 376-387.
von Caemmerer S., Ghannoum O., Pengelly J.J.L. & Cousins A.B. (2014) Carbon isotope discrimination as a tool to explore C4 photosynthesis. *Journal of Experimental Botany*, **65**, 3459-3470.
von Caemmerer S., Quick W.P. & Furbank R.T. (2012) The development of C4 rice: current progress and future challenges. *Science*, **336**, 1671-1672.
Walker B.J. & Ort D.R. (2015) Improved method for measuring the apparent CO2 photocompensation point resolves the impact of multiple internal conductances to CO2 to net gas exchange. *Plant, Cell & Environment*, n/a-n/a.
Wang Y., Long S.P. & Zhu X.-G. (2014) Elements Required for an Efficient NADP-Malic Enzyme Type C4 Photosynthesis. *Plant Physiology*, **164**, 2231-2246.
Yamori W. & von Caemmerer S. (2009) Effect of Rubisco Activase Deficiency on the Temperature Response of CO2 Assimilation Rate and Rubisco Activation State: Insights from Transgenic Tobacco with Reduced Amounts of Rubisco Activase. *Plant Physiology*, **151**, 2073-2082.
Yin X., Belay D., van der Putten P.L. & Struik P. (2014) Accounting for the decrease of photosystem photochemical efficiency with increasing irradiance to estimate quantum yield of leaf photosynthesis. *Photosynthesis Research*, **122**, 323-335.
Yin X., Struik P.C., Romero P., Harbinson J., Evers J.B., Van Der Putten P.E.L. & Vos J.A.N. (2009) Using combined measurements of gas exchange and chlorophyll fluorescence to estimate parameters of a biochemical C3 photosynthesis model: a critical appraisal and a new integrated approach applied to leaves in a wheat (Triticum aestivum) canopy. *Plant, Cell & Environment*, **32**, 448-464.
Yin X., Sun Z., Struik P.C. & Gu J. (2011a) Evaluating a new method to estimate the rate of leaf respiration in the light by analysis of combined gas exchange and chlorophyll fluorescence measurements. *Journal of Experimental Botany*, **62**, 3489-3499.
Yin X., Van Oijen M. & Schapendonk A. (2004) Extension of a biochemical model for the generalized stoichiometry of electron transport limited C3 photosynthesis. *Plant, Cell & Environment*, **27**, 1211-1222.
Yin X.Y. & Struik P.C. (2012) Mathematical review of the energy transduction stoichiometries of C4 leaf photosynthesis under limiting light. *Plant Cell and Environment*, **35**, 1299-1312.
Yin X.Y., Sun Z.P., Struik P.C., Van der Putten P.E.L., Van Ieperen W. & Harbinson J. (2011b) Using a biochemical C4 photosynthesis model and combined gas exchange and chlorophyll fluorescence measurements to estimate bundle-sheath conductance of maize leaves differing in age and nitrogen content. *Plant Cell and Environment*, **34**, 2183-2199.

Table 1. Acronyms, definitions, variables, and units used.

Symbol	Definition	Values / Units / References
A	Measured net assimilation	µmol m^{-2} s^{-1}
A_{MOD}, A_C	Net assimilation under ambient O_2 modelled through Eqn 3 and 14 respectively	µmol m^{-2} s^{-1}
A_{SAT}	CO_2–saturated *A*, under the PPFD of *A*/*Ci*-curves	µmol m^{-2} s^{-1}
b	*y*–intercept of the linear fit of *Y(II)* against *Y(CO₂)*, it represent the fraction of *Y(II)* not used for PEP regeneration, RPP and PCO cycles, i.e. the fraction of *Y(II)* used by alternative ATP sinks	dimensionless (Valentini *et al.*, 1995)
BS	Bundle Sheath	
C_a	CO_2 concentration in the cuvette as measured by the GES	µmol mol^{-1}
C_{BS}	CO_2 concentration in the BS (Eqn 20 and 22)	µmol mol^{-1}
CCM	Carbon Concentrating Mechanism	
CE	Carboxylating efficiency, i.e. initial slope of the *A*/C_i curve	mol m^{-2} s^{-1}
C_i	CO_2 concentration in the substomatal cavity as calculated by the GES	µmol mol^{-1} (Eqn 1–18 in the LI–COR 6400 manual)
C_M	CO_2 concentration at the site of PEPC carboxylation $C_M = C_i - \frac{A}{g_M}$	µmol mol^{-1}
EFT	Excel based Fitting Tool	
F	Photorespiration rate, or rate of photorespiratory CO_2 evolution $F = 0.5 \cdot V_O$	µmol m^{-2} s^{-1}
F	Chlorophyll *a* fluorescence signal (corresponding to fluorescence yield because normalized to measuring light)	dimensionless
GA	Gross assimilation $GA = A + R_{LIGHT}$. *GA* represents the net biochemical CO_2 uptake *GA*=V_C-*F*	µmol m^{-2} s^{-1}
GA_{MOD}	Gross assimilation under ambient or low O_2 modelled through Eqn 3	µmol m^{-2} s^{-1}
GA_{SAT}	Light–saturated *GA*, under the CO_2 concentration of light–curves	µmol m^{-2} s^{-1}
g_{BS}	BS conductance to CO_2 diffusion	mol m^{-2} s^{-1}
g_M	Mesophyll conductance to CO_2 diffusion	mol m^{-2} s^{-1}
GES	Portable Fluorescence–Gas Exchange systems	
J_{ATP}	ATP production rate used by PEP regeneration (C_4 cycle), RPP and PCO cycles	µmol m^{-2} s^{-1}
J_{ATPSAT}	Light–saturated ATP production rate, Eqn 11	µmol m^{-2} s^{-1}
J_{ATPMOD}	Modelled J_{ATP}, either empirically through Eqn 11 ($J_{ATPMOD\ Emp}$), or mechanistically through Eqn 12 ($J_{ATPMOD\ Mech.}$)	µmol m^{-2} s^{-1}
k	GES cuvette diffusion correction parameter	mol/s
k'	Slope of the linear fit of *Y(II)* against *Y(CO₂)*, Eqn 5	dimensionless (Valentini *et al.*, 1995)
K_C	Rubisco Michaelis–Menten constant for CO_2	650 µbar (von Caemmerer, 2000)
K_O	Rubisco Michaelis–Menten constant for O_2	450000 µbar (von Caemmerer, 2000)
K_P	PEPC Michaelis–Menten constant for CO_2	80 µbar or variable (von Caemmerer, 2000)
L	Leak rate, i.e. magnitude of CO_2 flux diffusing out of BS, Eqn 21	µmol m^{-2} s^{-1}
LCP	Light compensation point, i.e. *PPFD* when *A*=0. At the *LCP* the rate of Rubisco carboxylation equals the rate of respiration + photorespiratory CO_2 release (V_C=R_{LIGHT}+*F*). In non–photorespiratory conditions, when V_C=R_{LIGHT}, the *LCP* is lower.	µmol m^{-2} s^{-1}
M	Mesophyll	
O_M, O_{BS}	O_2 concentration in M cells (assumed to equal ambient) or BS cells (Eqn 23)	O_M = 210000 µmol mol^{-1}
PCO	Photosynthetic Carbon Oxygenation (cycle)	
PEP	Phosphoenolpyruvate	
PEPC	Phosphoenolpyruvate carboxylase	
PEPCK	Phosphoenolpyruvate carboxykinase	
PGA	3–phosphoglyceric acid	
PPFD	Photosynthetic Photon Flux Density	µmol m^{-2} s^{-1}
$PPFD_{50}$	*PPFD* which half saturates either *GA* or *J*	µmol m^{-2} s^{-1}
PSII	Photosystem II	
R_{DARK}	Dark respiration	R_{DARK} >0 µmol m^{-2} s^{-1}
R_{LIGHT}	Respiration in the light; also known as non–photorespiratory CO_2 release in the light, or respiration in the day	R_{LIGHT} >0 µmol m^{-2} s^{-1}
R_M	M fraction of R_{LIGHT}	generally 0.5 R_{LIGHT}
RPP	Reductive pentose phosphate (cycle); also known as Calvin–Benson–Bassham cycle or photosynthetic carbon reduction cycle	
Rubisco	Ribulose bisphosphate carboxylase oxygenase	
RuBP	Ribulose–1,5–bisphosphate	
s'	A calibration factor to calculate J_{ATP} according to Yin, it depends on leaf absorptance, PSII optical cross section, accounts for engagement of alternative electron sinks and cyclic electron flow, and the stoichiometry of ATP synthase	dimensionless (Yin *et al.*, 2004)
V_C	Rubisco carboxylation rate, Eqn 16	µmol m^{-2} s^{-1}
V_{CMAX}	CO_2–saturated Rubisco carboxylation rate	60 µmol m^{-2} s^{-1} (von Caemmerer, 2000)
V_{PMAX}	PEPC carboxylation rate, Eqn 15	µmol m^{-2} s^{-1}
V_P	CO_2–saturated PEPC carboxylation rate	µmol m^{-2} s^{-1}
V_O	Rubisco oxygenation rate (Eqn 18)	µmol m^{-2} s^{-1}
x	Factor partitioning J_{ATP} between PEP regeneration (C_4 activity) and RPP+PCO cycle (C_3 activity), Eqn 15 and 16	generally 0.4 but can vary (Kromdijk *et al.*, 2010)
Y(CO₂)	Quantum yield for CO_2 fixation $Y(CO_2) = \frac{GA}{PPFD}$; also known as Φ_{CO2}	dimensionless
$Y(CO_2)_{LL}$	Initial (or maximum) quantum yield for CO_2 fixation, i.e. quanta required for each CO_2 assimilated; Φ_{CO2LL} in the notation of Yin	
Y(II), $Y(II)_{AMB}$,	Yield of photosystem II, $Y(II) = \frac{F'_M - F_S}{F'_M}$; also known as Φ_2 or Φ_{PS2}, unspecified, under ambient or low O_2	dimensionless (Genty *et al.*, 1989)

$Y(II)_{LOW}$	respectively	
$Y(II)_{LL}$	Initial *Y(II)* extrapolated to *PPFD*=0	dimensionless
$Y(J_{ATP})_{LL}$	Initial (or maximum) quantum yield for ATP production, i.e. conversion efficiency of *PPFD* into J_{ATP} (Eqn 6 and 7)	dimensionless
α	Fraction of PSII active in BS	dimensionless
Γ	C_i–A compensation point, i.e. C_i at which A=0 and V_C=R_{LIGHT}+F	µmol mol^{-1}
γ*	Half the reciprocal Rubisco specificity $\gamma* = \frac{1}{2S_{C/O}}$	0.000193 (von Caemmerer, 2000)
θ	Curvature of the non–rectangular hyperbola describing the *PPFD* dependence of J, Eqn 11	dimensionless
ω	Curvature of the non–rectangular hyperbola describing the C_i dependence of A, Eqn 3	dimensionless
m	Curvature of the non–rectangular hyperbola describing the *PPFD* dependence of *GA*, Eqn 2	dimensionless
ϕ	Leakiness, ϕ=L/V_P	dimensionless

Table 2. Minimum data required to obtain a desired output

Desired output	Minimum data necessary	Notes
s'	Low O_2 fluorescence–light–response curve	
k′, b	R_{LIGHT}, low O_2 fluorescence–A/C_i response curve or low O_2 fluorescence–light–response curve	If both curves are available they can be pooled
$Y(CO_2)_{LL}$, LCP, GA_{SAT}, $PPFD_{50}$ (GA)	Light–response curve, R_{LIGHT}	If R_{LIGHT} is not available it can be derived in the same fitting
J_{ATPSAT}, $PPFD_{50}$ (J_{ATP})	Fluorescence–light–response curve, s' or k′ and b	
$Y(II)_{LL}$	Fluorescence–light–response curve	
$Y(J_{ATP})_{LL}$	$Y(II)_{LL}$, s' or k′ and b	
K_P and V_{PMAX}	A/C_i response curve, R_{LIGHT}, g_{BS}	Values for O_M, α, g_M, γ*, x, R_M/R_{LIGHT}, Rubisco kinetic constants K_C, K_O, V_{CMAX} are assumed (Table 1)
Γ, CE, A_{SAT}, C_{i50}, L_S	A/C_i response curve	
LCP	Light–response curve	R_{LIGHT} is preferably required if LCP is derived non–linearly (together with GA_{SAT})
g_{BS}	Fluorescence–light response curve, R_{LIGHT}, s' or k′ and b	Values for O_M, α, g_M, γ*, x, R_M/R_{LIGHT} are assumed
R_{LIGHT}	Fluorescence–light–response curve	If fluorescence data are not available R_{LIGHT} can be estimated in Sheet 4 by non–linear curve fitting
V_C, V_O, F	A and $Y(II)$ for each desired datapoint, R_{LIGHT}, s' or k′ and b	
C_M, C_{BS}, L, ϕ	A, C_i, and $Y(II)$ for each desired datapoint, g_{BS}, s' or k′ and b, R_{LIGHT}	Values for g_M, x, R_M/R_{LIGHT} (mass balance) and O_M, α, γ* (Rubisco specificity) are assumed

Table 3. Output obtained by analysing the primary responses of maize plants reported in Figure 1. n=3. †additional output, ‡methodological variants.

				Ambient O_2			Low O_2		
Logical Step	Output	Unit	Method	Mean	C.V. / %	EFT Location sheet, cell	Mean	C.V. / %	EFT Location sheet, cell
2	R_{LIGHT}	µmol m^{-2} s^{-1}	Fluorescence–Light (Yin)	1.45	11	2–3, N6	1.47	11	2–3, P6
3	$Y(II)_{LL}$	dimensionless	Linear	0.726	1	2–3, N7 (AR11)	0.716	1	2–3, P7 (AT11)
4	LCP	µmol m^{-2} s^{-1}	Hyperbola	28.2	13	4a, G5	26.5	16	4b, G5
4	GA_{SAT}	µmol m^{-2} s^{-1}	Hyperbola	30.8	8	4a, M3	32.7	7	4b, M3
4	$Y(CO_2)_{LL}$	CO_2/quanta	Hyperbola	0.0520	8	4a, M2	0.0562	6	4b, M2
4	$PPFD_{50}$	µmol m^{-2} s^{-1}	Hyperbola	328	3	4a, G6	335	4	4b, G6
4	m	dimensionless	Hyperbola	0.889	6	4a, M4	0.849	6	4b, M4
5	CE	mol m^{-2} s^{-1}	Hyperbola	0.640	14	5a M2	0.602	8	5b M2
5	A_{SAT}	µmol m^{-2} s^{-1}	Hyperbola	34.4	17	5a M3	35.5	11	5b M3
5	ω	dimensionless	Hyperbola	0.717	25	5a M4	0.737	14	5b M4
5	Γ	µmol m^{-2} s^{-1}	Hyperbola	0	–	5a M5	0	–	5b M5
5	C_{i50}	µmol m^{-2} s^{-1}	Hyperbola	34.5	20	5a G3	37.3	14	5b G3
5	L_S	dimensionless	Hyperbola	0.161	41	5a Z15†	0.179	27	5b Z15†
6	s'	CO_2/quanta	Yin	–	–	–	0.237	5	6a–7, M5
6	k'	quanta/CO_2	*Valentini*	–	–	–	7.47	5	6b–7, G5
6	b	dimensionless	*Valentini*	–	–	–	0.281	5	6b–7, G6
7	$Y(J_{ATP})_{LL}$	ATP/quanta	*Valentini*	0.298	5	6b–7, G9‡	0.292	6	6b–7, G10‡
9	J_{ATPSAT}	µmol m^{-2} s^{-1}	*Valentini*	167	9	8–9, M2‡	–	–	–
9	θ	dimensionless	*Valentini*	0.858	9	8–9, M3‡	–	–	–
9	$PPFD_{50}$	µmol m^{-2} s^{-1}	*Valentini*	328	8	8–9, M6‡	–	–	–
10	g_{BS}	mol m^{-2} s^{-1}	J_{ATP} from Valentini	0.00123	9	10, R7‡	–	–	–
11	V_{PMAX}	µmol m^{-2} s^{-1}	g_{BS} from J_{ATP} Valentini	82.8	11	11a, Q7‡	76.7	8	11b, Q7‡

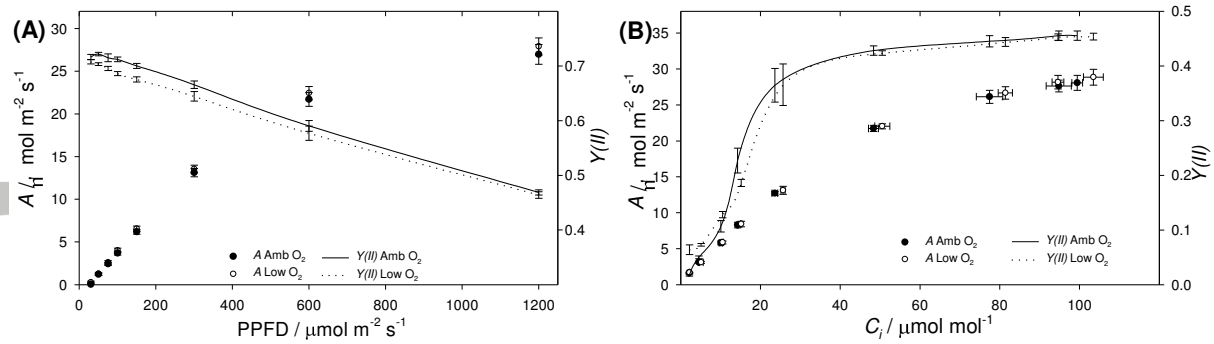

Figure 1. Example of fluorescence – gas exchange data obtained on maize plants. Panel **A**: light–response curves. Symbols show the response of A to increasing PPFD measured under ambient O_2 (closed circles) or 2% O_2 (open circles). Lines show the response of Y(II) under ambient O_2 (solid line) or 2% O_2 (dotted line). Mean ± SE. Panel **B**: A/C_i response curves. Symbols show mean A ± SE plotted against mean C_i ± SE measured under ambient O_2 (closed circles) or 2% O_2 (open circles). Lines show mean Y(II) ± SE for the same datapoints. n=3.

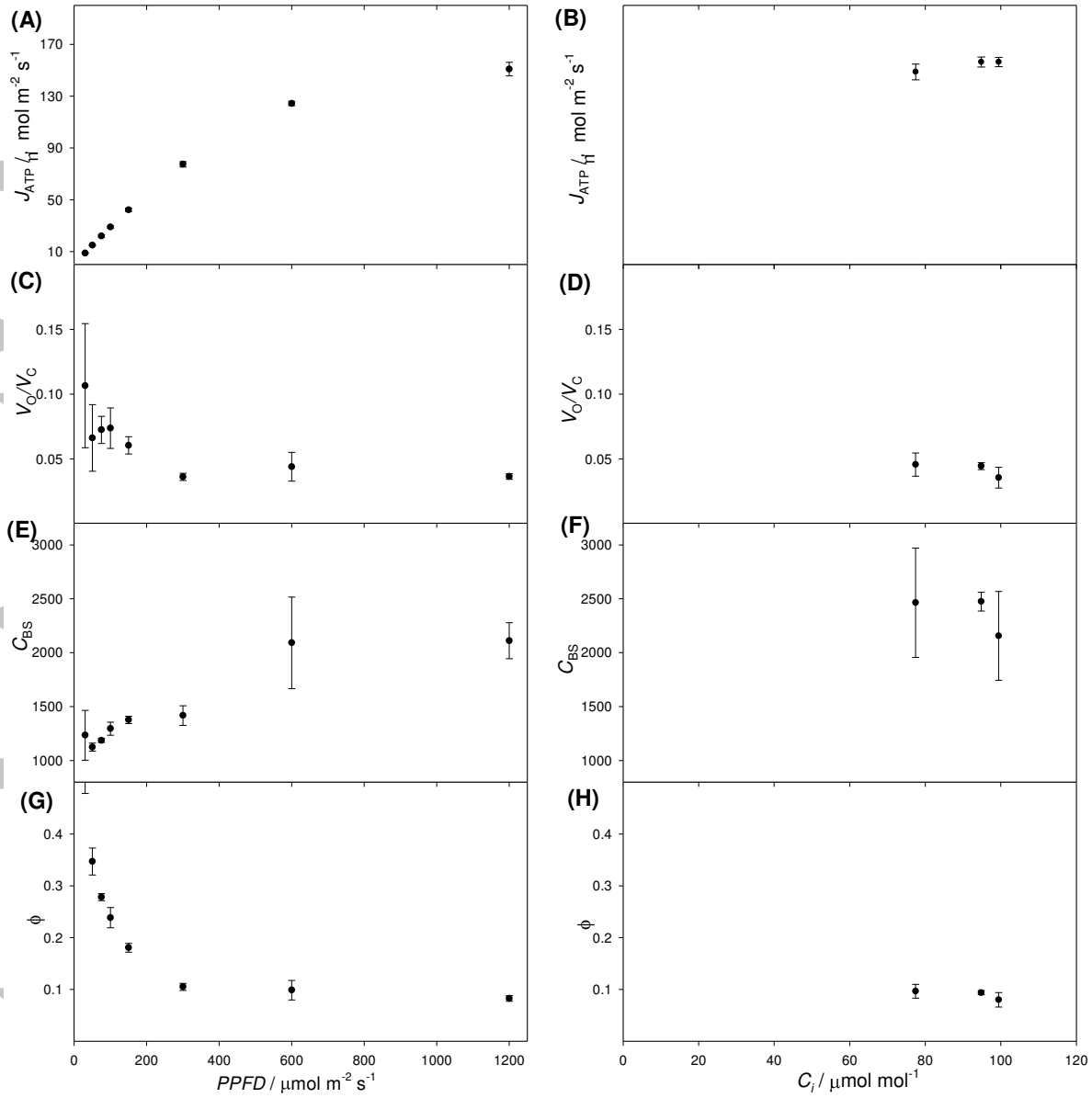

Figure 2. Example of output obtained on maize plants. Panel **A**: J_{ATP} calculated for light–response curves obtained with the Valentini calibration. Panel **B**: J_{ATP} calculated for A/C_i response curves. Because the Valentini calibration was performed on light–limited datapoints, only light limited datapoints are shown. Panel **C**: V_O/V_C calculated for light–response curves using the values of J_{ATP} shown in panel A. Panel **D**: V_O/V_C calculated for A/C_i response curves using the values of J_{ATP} shown in panel B. CO_2 concentration in BS (C_{BS}) calculated for light–response curves (Panel **E**) and for A/C_i response curves (Panel **F**) using the values of J_{ATP} shown in panel A and B. Bundle sheath leakiness ϕ calculated for light–response curves (Panel **G**) and for A/C_i response curves (Panel **H**) using the values of J_{ATP} shown in panel A and B. Mean ± SE; n=3.